HHS Public Access

Author manuscript

J Nucl Med. Author manuscript; available in PMC 2017 March 27.

Published in final edited form as:

J Nucl Med. 2015 July ; 56(7): 1042–1047. doi:10.2967/jnumed.114.151480.

Voxel-wise relationships between distribution volume ratio and cerebral blood flow: implications for analysis of β-amyloid images

Jitka Sojkova[1], **Joshua Goh**[1,2], **Murat Bilgel**[1,3], **Bennett Landman**[4], **Xue Yang**[4], **Yun Zhou**[5], **Yang An**[1], **Lori L. Beason-Held**[1], **Michael A. Kraut**[5], **Dean F. Wong**[5,6,7,8], and **Susan M. Resnick**[1]

[1]Laboratory of Behavioral Neuroscience, National Institute on Aging, NIH

[2]National Taiwan University

[3]Department of Biomedical Engineering, Johns Hopkins University

[4]Department of Electrical Engineering, Vanderbilt University

[5]Russell H. Morgan Department of Radiology and Radiological Sciences, Johns Hopkins University

[6]Department of Psychiatry and Behavioral Sciences, Johns Hopkins University

[7]Solomon Snyder Department of Neuroscience, Johns Hopkins University

[8]Environmental Health Sciences, Johns Hopkins University

Abstract

Quantification of β-amyloid (Aβ) in vivo is often accomplished using the distribution volume ratio (DVR), based on a simplified reference tissue model. We investigated the local relationships between DVR and cerebral blood flow (CBF), as well as relative blood flow (R_1), in nondemented older adults.

Methods—Fifty-five nondemented participants (mean age 78.5 years) in the Baltimore Longitudinal Study of Aging underwent ^{15}O-H_2O PET CBF and dynamic ^{11}C-PiB-PET. ^{15}O-H_2O PET images were normalized and smoothed using SPM. A simplified reference tissue model with linear regression and spatial constraints was used to generate parametric DVR images. The DVR images were regressed on CBF images on a voxel-by-voxel basis using robust Biological Parametric Mapping, adjusting for age and sex (FDR p=0.05, k=50). DVR images were also regressed on R_1 images, a measure of the transport rate constant from vascular space to tissue. All analyses were performed in the entire sample, and in high and low tertiles of mean cortical DVR.

Results—Voxel-based analyses showed that increased DVR is associated with increased CBF in frontal, parietal, temporal, and occipital cortices. However, this association appears to spare regions that typically show early β-amyloid (Aβ) deposition. A more robust relationship between DVR and CBF was observed in the lowest tertile of DVR, i.e., negligible cortical Aβ load,

Send Correspondence to: Susan M. Resnick, Ph.D. Laboratory of Behavioral Neuroscience, Biomedical Research Center, National Institute on Aging, IRP, 251 Bayview Blvd. Room 4B335, Baltimore, MD 21224, Phone: 410-558-8618, resnicks@mail.nih.gov.

compared to the highest tertile of cortical DVR and Aβ load. Spatial distributions of the DVR-CBF and DVR-R_1 correlations showed similar patterns. No reliable negative voxel-wise relationships between DVR and CBF or R_1 were observed.

Conclusion—Robust associations between DVR and CBF at negligible Aβ levels, together with similar spatial distributions of DVR-CBF and DVR-R_1 correlations, suggest that regional distribution of DVR reflects blood flow and tracer influx rather than pattern of Aβ deposition in those with minimal Aβ load. DVR-CBF associations in individuals with higher DVR are more likely to reflect true associations between patterns of Aβ deposition and CBF or neural activity. These findings have important implications for analysis and interpretation of voxel-wise correlations with external variables in individuals with varying amounts of Aβ load.

Keywords

Amyloid; cerebral blood flow; PiB; aging; DVR

Introduction

Since the initial visualization of β-amyloid (Aβ) in vivo(1), a number of studies have investigated Aβ deposition in nondemented older adults using ^{11}C-Pittsburgh compound B (PiB) (2-6). Accurate quantification of Aβ is especially important in this population, where associations with other biomarkers and individual differences in cognition and genetic, metabolic, and other medical covariates may enhance understanding of the pathophysiology and temporal sequence of changes in Alzheimer's disease (AD), including the timing of Aβ deposition in relation to changes in brain structure and function (7).

An inverse association between Aβ deposition and regional cerebral glucose metabolism has been demonstrated in AD (1, 8, 9). However, recent findings suggest that deficits in cerebral glucose metabolism, measured by PET-fluorodeoxyglucose (FDG), may not always match the regional distribution of Aβ deposition. For example, in atypical clinical variants of AD, such as the logopenic variant of primary progressive aphasia and posterior cortical atrophy, the pattern of glucose hypometabolism is consistent with the clinical presentation of these AD variants despite similarly widespread Aβ deposition by the time of clinical diagnosis (10). The association between Aβ deposition and glucose metabolism is even less clear in nondemented older adults, with studies yielding conflicting results (11-13). Due to considerations of participant burden and cost, it is not always feasible to perform ^{11}C-PiB-PET and ^{18}F-FDG studies in the same individuals. ^{15}O-H_2O PET measures of regional cerebral blood flow (CBF) provide an alternate approach for investigation of regional brain function that is more readily integrated with a ^{11}C-PiB-PET study due to the short ^{15}O half-life and imaging durations.

In addition, dynamic acquisition of ^{11}C-PiB-PET studies allows estimation of parameters that may reflect both Aβ and CBF. For example, the simplified reference tissue model with linear regression and spatial constraint (SRTM-LRSC) (14) provides estimates of the distribution volume ratio (DVR) for detection of Aβ and an estimate of R_1 or relative CBF flow. R_1 is the target to reference tissue ratio of the tracer transport rate constant from vascular space to tissue (K_1/K_{1ref})(14) and correlates well with regional cerebral glucose

metabolism, measured by ^{18}F-FDG PET (15). As such, R_1 can be used to enhance our understanding of the relationship between regional brain function and Aβ deposition in nondemented older adults where ^{18}F-FDG PET is not obtained.

In this study, we first investigated the voxel-wise association of ^{11}C-PiB-PET measures of Aβ deposition with concurrently acquired CBF measurements obtained from ^{15}O-H_2O PET in nondemented participants in the Baltimore Longitudinal Study of Aging. Next, we used the same approach to examine the relationship between the DVR measure of Aβ burden and the R_1 estimate of CBF based on the same ^{11}C-PiB-PET dynamic studies. We hypothesized that in nondemented older adults, DVR would be positively correlated with CBF and that this relationship would vary with the spatial distribution of Aβ deposition. Secondly, we expected that spatial patterns of associations between DVR and R_1 would parallel those between DVR and ^{15}O-H_2O measures of CBF.

Materials and Methods

Participants

Participants were 55 nondemented adults (mean age 78.5, SD 6.3 yrs.) from the Neuroimaging substudy of the Baltimore Longitudinal Study of Aging (NI-BLSA) (16), who underwent ^{11}C-PiB-PET and resting ^{15}O-H_2O PET on the same day. Seven of the participants had a Clinical Dementia Rating Scale (CDR)(17) score of 0.5, three of whom met consensus conference-based criteria for mild cognitive impairment (MCI) at the time of study. Consensus diagnosis followed established procedures (18, 19) and was based on serial neuropsychological evaluations and the CDR scale, which was typically informant-based. The neuropsychological measures used for consensus diagnosis included tests of mental status, word knowledge and verbal ability, memory, language, verbal fluency, attention, executive function, and visuospatial ability. MCI was diagnosed in participants with progressive decline in a single cognitive domain or more than a single domain with absence of documented functional impairment. Diagnosis of dementia followed Diagnostic and Statistical Manual of Mental Disorders III-R criteria(20), and diagnosis of AD was based on the National Institute of Neurological and Communicative Disorders and Stroke–Alzheimer's Disease and Related Disorders Association criteria(21). Exclusionary criteria included stroke or head trauma. Sample characteristics are shown in Table 1.

This study was approved by the Institutional Review Boards of the NIA Intramural Research Program and the Johns Hopkins Medical Institutions. Written informed consent was obtained from each participant at each visit.

^{11}C-PiB-PET Image Acquisition and Processing

Dynamic ^{11}C-PiB-PET studies were performed on a GE Advance scanner in 3D mode, and 33 time frames (70 min acquisition) were obtained. Image acquisition started immediately after intravenous bolus injection of mean (SD) 14.58 (0.81) mCi ^{11}C-PiB with specific activity of 5.56 (2.98) Ci/μmol. Participants were fitted with a thermoplastic mask to minimize motion during scanning. Transmission scans in 2D mode using a Ge-68 source were used for attenuation correction. Dynamic images were reconstructed using filtered back

projection with a ramp filter (image size=128×128, pixel size=2×2mm, slice thickness=4.25mm), yielding a spatial resolution of about 4.5mm FWHM at the center of field of view.

MRI scans, co-registered to the corresponding ^{11}C-PiB-PET, were used for definition of regions of interest. Spoiled gradient recalled (SPGR) or MPRAGE MRI scans (124 slices, image matrix=256×256, pixel size=0.94×0.94mm, slice thickness=1.5 mm) were coregistered to the mean of the first 20 min dynamic PET images for each participant using the mutual information method in the Statistical Parametric Mapping software (SPM2; Wellcome Department of Cognitive Neurology, London, England). With the exception of one claustrophobic participant whose structural MRI was obtained 10 years prior to the initial ^{11}C-PiB-PET assessment, participants had structural MRI scans within 3 years of each ^{11}C-PiB-PET study. The cerebellar gray ROI, which was used as the reference region, was manually drawn on the MRI and then applied to the ^{11}C-PiB-PET scans. In addition to cerebellum, fifteen ROI's were manually drawn on the co-registered MRIs to sample the PET radioactivity(14, 22).

Parametric DVR images were generated by simultaneous fitting of a reference tissue model with spatial constraint (SRTM-LRSC) to dynamic ^{11}C-PiB-PET images(14, 23). DVR values for the 15 ROIs were then extracted from the parametric images. Mean cortical DVR (cDVR) was calculated by averaging DVR values from orbitofrontal, prefrontal (including middle and inferior frontal gyri), superior frontal, parietal, lateral temporal, occipital, and anterior and posterior cingulate regions. Parametric images were then spatially normalized using an R_1 ($=K_1/K_1$(reference tissue), the target to reference tissue ratio of tracer transport rate constant from vascular space to tissue) template (14) and smoothed with a Gaussian filter of 8, 8, 8 mm in the x, y, and z planes. We defined minimal cDVR as values below DVR = 1.062, based on the test/retest variability for DVR using SRTM analysis of +/-6.2%(24) and the fact that DVR = 1 was considered as the absence of specific binding.

^{15}O-H_2O PET Acquisition and Image Processing

Resting state ^{15}O-H_2O scans were acquired on a GE Advance PET scanner in 3D mode. Images were obtained for 60 seconds once the total radioactivity counts in brain reached threshold levels, as described previously(25). A transmission scan in 2D mode utilizing a Ge-68 rotating source was used for attenuation correction. ^{15}O-H_2O scans were performed after the transmission scan and before the ^{11}C-PiB-PET scan with 10 minutes between scans.

Using Statistical Parametric Mapping (SPM5; Wellcome Department of Imaging Neuroscience, London, England), ^{15}O-H_2O PET scans were spatially normalized into standard stereotaxic space and smoothed using a Gaussian kernel to a full width at half maximum of 10, 10, and 10 mm in the x, y, and z planes. To control for variability in global flow, rCBF values at each voxel were ratio-adjusted to the mean global flow and scaled to 50 ml/100g/min for each image.

Voxel-wise relationship of DVR with CBF and R_1

We used Robust Biological Parametric Mapping (BPM), version 2.1(26, 27), to determine voxel-wise DVR-CBF and DVR-R_1 relationships. Robust BPM is based on BPM, which allows voxel-wise regression of data from two imaging modalities using least-squares regression.(28) Robust BPM extends this approach by using robust regression (M-estimation) (29) to account for outliers in the imaging data (26).

We first regressed DVR images on globally adjusted CBF images, using age and sex as covariates, in the entire sample of 55 participants. We then repeated the regression analyses for the upper (n=18) and lower (n=18) tertiles defined by cDVR. Subsequently, we regressed DVR images on R_1 images, using age and sex as covariates, both in the whole group and in the upper and lower tertiles defined by cDVR. Significant effects for all analyses were generated with FDR correction at p=0.05 and spatial extent >50 voxels.

Results

Cortical ^{11}C-PiB retention

The distribution of cDVR by tertile is shown in Figure 1. The cDVR means were 1.17 (SD 0.26) for the entire sample, 0.93 (SD 0.02, range 0.89- 0.97) in the lowest tertile, and 1.49 (SD 0.16, range 1.25-1.76) in the highest tertile. The DVR values for the 9 cortical ROIs comprising the cDVR are presented in Table 2 for the whole sample, as well as the upper and lower tertile subgroups. As expected from the subgroup definition, upper and lower tertiles showed significant differences for cDVR and regional DVRs ($p<0.005$).

Association between DVR and ^{15}O-H_2O CBF

In the entire sample, only positive correlations were observed between DVR and CBF using a conservative threshold of FDR=0.05, with a spatial extent of 50 voxels. With higher DVR and greater amyloid burden, higher CBF was seen in frontal (left superior and left middle frontal gyrus), parietal (bilateral paracentral lobule and postcentral gyri, right superior parietal lobule), temporal (bilateral superior and right inferior temporal gyri, and bilateral uncus), and occipital (right cuneus) cortex as well as bilateral thalamus, right midbrain, and bilateral cerebellum (Supplemental Table 1). Of the cortical structures, the largest spatial extent (4772 voxels) and T-value (11.16) localized to the paracentral lobule. Figure 2A illustrates DVR-CBF relationships in the paracentral lobule, with extension primarily anterior to the medial frontal gyrus. Importantly, DVR was not related to CBF in orbitofrontal gyrus, the majority of cingulate gyrus or precuneus although these regions have moderate to high amounts of Aβ (Table 2). Nevertheless, there are also regions, such as the superior frontal gyrus, which have elevated DVR (1.2 SD 0.34) and do show association between DVR and CBF. Interestingly, the medial temporal gyrus, which has very low DVR (1.01 SD 0.09) showed robust voxel-wise relationships between DVR and CBF.

We next investigated the relationship between DVR and CBF by cDVR tertile. We found that higher DVR is associated with higher CBF in the upper tertile subgroup. These findings localized to the frontal (left superior, middle, and orbitofrontal gyri, right medial and inferior frontal gyri, and bilateral subcallosal gyrus), parietal (right paracentral lobule), temporal

(bilateral superior and left middle temporal gyrus, right fusiform gyrus, and left insula), and occipital (left middle occipital gyrus and left cuneus) lobes, as well as right cingulate gyrus, left caudate, and right cerebellum (Supplemental Table 1). The greatest spatial extent (1237 voxels) with a T-value of 16.61 was observed in the right paracentral lobule. Figure 2A shows associations between DVR and CBF in the medial frontal gyrus and the paracentral lobule for the upper cDVR tertile.

DVR-CBF analysis in the lowest tertile group showed greater spatial extent than in the upper tertile group (Figure 2A). DVR-CBF correlations localized to the frontal (bilateral superior, and right inferior frontal gyrus as well as left precentral gyrus), parietal (right inferior parietal lobule), and temporal (right superior, middle, and inferior temporal gyri, right fusiform gyrus, and right uncus) cortex, as well as corpus callosum and cerebellum (Supplemental Table 1). Of these regions, the corpus callosum had the greatest spatial extent (19901 voxels) and T-value (20.24).

A number of DVR-CBF associations were in common across analyses for the upper and lower cDVR tertile subgroups. These include left superior and inferior frontal gyri, right superior and middle temporal gyri, and right cingulate gyrus.

Association between DVR and R_1

Similar to the findings for associations between DVR and ^{15}O-H_2O CBF in the entire sample, only positive correlations between DVR and R_1 reached the statistical threshold. Correlations between DVR and R_1 localized to similar regions as DVR and CBF correlations, involving the frontal, parietal, temporal, and occipital cortices as well as cerebellum (Figure 2B, Supplemental Table 2). The largest extent of DVR-R_1 correlation localized to the medial frontal gyrus, paracentral lobule, and cerebellum.

In addition, we also investigated DVR and R_1 by cDVR tertiles. In both the upper and lower cDVR tertile subgroups, only positive associations between R_1 and DVR were observed (Figure 2B). In the upper tertile, DVR-R_1 associations localized to the medial frontal gyrus, paracentral lobule, thalamus as well as cerebellum, and the spatial distribution of DVR-R_1 associations was similar to but of greater spatial extent than DVR-CBF associations. As compared to the upper tertile, the lowest tertile subgroup had greater spatial extent of DVR-R_1 associations, and these associations involved most of the frontal, parietal, temporal, and occipital cortex, as well as thalamus and cerebellum. In the lowest tertile group, the spatial extent of the DVR-R_1 associations was greater than that of DVR-CBF associations.

Discussion

Our voxel-wise analysis of ^{15}O-H_2O and ^{11}C-PiB-PET in nondemented older adults revealed that positive relationships between local DVR and CBF are less pronounced in many regions that typically have high Aβ deposition. Overall, individuals with low Aβ load demonstrate more robust relationships between DVR and CBF than those with high Aβ load. Furthermore, associations between DVR and R_1 show patterns similar to those between DVR and ^{15}O-H_2O CBF. Specifically, individuals with low DVR and low levels of Aβ demonstrate more robust DVR-R_1 relationships compared to those with high Aβ load.

Together, these findings suggest that at low DVR levels, regional patterns in DVR images reflect blood flow and tracer influx to tissue rather than patterns related to Aβ deposition.

We found significant positive but no inverse associations between DVR and CBF in individuals without clinical diagnoses of dementia. The spatial distribution of this DVR-CBF relationship with respect to the distribution of Aβ load provides insight for understanding the DVR-CBF associations. Higher DVR is related to higher CBF in frontal, parietal, temporal, and occipital cortices, with the greatest spatial extent in the paracentral lobule extending anteriorly to the medial frontal gyrus. However, regions with early Aβ deposition, such as precuneus, do not show extensive and robust associations between DVR and CBF. This suggests that there may be factors other than increased Aβ load that underlie the DVR-CBF relationships in the regions showing extensive associations in the sample as a whole.

To further investigate this, we examined the effect of Aβ load, measured by mean cDVR, on the relationship between DVR and CBF. We found that both magnitude and spatial extent of DVR-CBF relationships were greater in the lowest tertile group with negligible or low Aβ load. As in the analysis of the whole sample, regions that typically have high amounts of Aβ did not show extensive relationships between DVR and CBF. These findings suggest that DVR images, especially at low cDVR levels, likely represent patterns of cerebral blood flow and tracer delivery rather than Aβ deposition. We also found that the region in the low cDVR group with the highest spatial extent for DVR-CBF association is corpus callosum, consistent with delayed tracer clearance for PiB in white matter (30).

To understand directly the contribution of tracer influx to DVR, we also investigated the relationship between DVR and R_1. We found a robust relationship between DVR and R_1 at low cDVR levels, involving the majority of the cortex which contrasts with lesser spatial extent of DVR-R_1 associations at high cDVR levels. This suggests that DVR images at low cDVR levels, in addition to reflecting blood flow, also reflect tracer influx. Nevertheless, as can be seen from Figure 2B, even in the upper tertile, R_1 is related to DVR. Therefore, it is essential to determine the level of Aβ load at which DVR images represent regional patterns of Aβ deposition rather than blood flow or tracer influx. It is likely that differences in regional patterns of PiB retention at different levels of Aβ can be informative in this regard, as suggested by our recent report that spatial patterns of PiB retention and progression may be better markers of cognitive decline compared with cDVR alone (31). A clearer understanding of the extent to which tracer influx contributes to regional patterns of retention of PiB and other amyloid radiotracers will be important for both statistical analysis and clinical interpretation of amyloid imaging scans.

Both DVR-R_1 and DVR-CBF associations were positive in direction, and regression of R_1 on DVR localized to the medial frontal gyrus and the paracentral lobule, regions also showing DVR-CBF relationships. However, the DVR-R_1 associations showed greater spatial extent in comparison to the DVR-CBF associations. In part, the greater correspondence between DVR and R_1 may reflect correlated noise, because R_1, unlike independently assessed CBF, is used in the calculation of tissue concentration of the tracer (14). Our study extends the findings of Blomquist et al. who in a study of a rhesus monkey found that K_1

for ^{11}C-PiB reflects CBF (32). Here, we demonstrate similar, region specific, patterns of DVR-CBF and DVR-R_1 associations in humans.

Our study has important implications for interpretation of Aβ imaging data. Voxel-wise investigations of the relationship between local values of ^{11}C-PiB and external variables may be misleading given that DVR images at lower cDVR levels may not represent Aβ deposition but rather blood flow and tracer influx. Such analyses using genetic, cognitive, or other scalar data as covariates of interest assume that variation in regional distribution of tracer retention at both low and high levels reflects regional variation in Aβ deposition. As we have shown, the distribution of DVR values at different mean DVR levels can represent different processes. With values at higher cDVR levels reflecting regional patterns of Aβ deposition while those at lower cDVR levels representing regional patterns of blood flow and tracer influx, correlation or regression analyses including images across Aβ levels may lead to results that do not reflect a single biological process. While these findings are pertinent for investigations across diagnostic categories with a wide range of DVR values, they are perhaps more influential in nondemented older adults where a greater proportion of individuals with negligible levels of Aβ load might affect associations of DVR with external variables. On the other hand, this difference in the process underlying the spatial distribution of PiB retention at high and low overall levels of Aβ deposition may improve classification between cognitively stable and cognitive decliners (31). These findings further underscore the importance of investigating the DVR cutoff at which DVR images reflect other factors other than Aβ deposition.

In this study, we used robust BPM for DVR-CBF and DVR-R_1 voxel-wise correlations. An advance of robust BPM relative to BPM is its use of robust regression to reduce the effect of outliers which may be due to, for example, misregistration (33). In addition, we used SRTM to estimate DVR rather than the widely employed Logan graphical analysis approach, because SRTM allows simultaneous estimation of DVR and R_1. DVRs estimated by the Logan plot with reference tissue input are comparable to those estimated by SRTM at low noise levels of ROI kinetics but are underestimated in the presence of increased noise (23, 24). We also recognize that SUVR is commonly used for semi-quantitative measurement of PiB binding, due to simplified data acquisition and quantification, and note that highly linear correlations between DVR and SUVR were reported in previous studies with low noise levels of ROI kinetics (34-35). However, SUVR measurements are dependent on the time-window of acquisition (24, 34) and bias relative to DVR estimation is correlated with magnitude (35). Therefore, correlations of SUVR with CBF or R_1 will vary with time-window of acquisition and magnitude of amyloid-deposition.

Our study has several limitations. Our study was limited to individuals without clinical diagnoses of dementia. Further investigation of DVR-CBF and DVR-R_1 relationships in individuals with wider ranges of global DVR values such as seen in MCI or AD would allow for more direct evaluation of the cutoff of DVR values at which the regional patterns in the images are no longer heavily weighted by blood flow or tracer influx. In addition, while we have excluded individuals with stroke or head trauma, other contributing factors that may relate to vascular disease have not been considered. Nevertheless, our study has also several strengths. We studied individuals from the neuroimaging substudy of the BLSA, which

represents a well-characterized sample of nondemented older adults followed for 20 years (16). We used robust BPM which accounts for outliers to provide more accurate estimates of intermodality correlations.

Conclusion

We demonstrate that at low levels of global PiB retention, the regional pattern of DVR likely reflects blood flow and influx of the tracer to tissue, in addition to non-specific binding associated with tracer clearance. As such, studies investigating voxel-wise regional relationships between DVR and scalar values, as well as imaging data, might be limited in interpretation unless the correlational analysis is restricted to individuals with more than minimal tracer retention and Aβ load. On the other hand, differences in regional distribution of tracer retention at low and high levels of Aβ may aid in the discrimination of normal and impaired individuals.

Supplementary Material

Refer to Web version on PubMed Central for supplementary material.

Acknowledgments

We are grateful to the BLSA participants for their dedication to these studies. We also thank Wendy Elkins, MS and Beth Nardi, MA for study management, as well as the staff of the PET facility at Johns Hopkins University, and the neuroimaging staff of the NIA for their assistance. This research was supported by the Intramural Research Program of the NIH, National Institute on Aging, NIA Research and Development Contract HHSN260200400012C, and K24 DA000412 (DFW).

References

1. Klunk WE, Engler H, Nordberg A, et al. Imaging brain amyloid in Alzheimer's disease with Pittsburgh Compound-B. Ann Neurol. 2004; 55:306–319. [PubMed: 14991808]
2. Aizenstein HJ, Nebes RD, Saxton JA, et al. Frequent amyloid deposition without significant cognitive impairment among the elderly. Arch Neurol. 2008; 65:1509–1517. [PubMed: 19001171]
3. Mintun MA, Larossa GN, Sheline YI, et al. [11C]PIB in a nondemented population: potential antecedent marker of Alzheimer disease. Neurology. 2006; 67:446–452. [PubMed: 16894106]
4. Resnick SM, Sojkova J, Zhou Y, et al. Longitudinal cognitive decline is associated with fibrillar amyloid-beta measured by [11C]PiB. Neurology. 2010; 74:807–815. [PubMed: 20147655]
5. Rowe CC, Ellis KA, Rimajova M, et al. Amyloid imaging results from the Australian Imaging, Biomarkers and Lifestyle (AIBL) study of aging. Neurobiol Aging. 2010; 31:1275–1283. [PubMed: 20472326]
6. Villemagne VL, Burnham S, Bourgeat P, et al. Amyloid beta deposition, neurodegeneration, and cognitive decline in sporadic Alzheimer's disease: a prospective cohort study. Lancet Neurol. 2013; 12:357–367. [PubMed: 23477989]
7. Jack CR Jr, Knopman DS, Jagust WJ, et al. Tracking pathophysiological processes in Alzheimer's disease: an updated hypothetical model of dynamic biomarkers. Lancet Neurol. 2013; 12:207–216. [PubMed: 23332364]
8. Edison P, Archer HA, Hinz R, et al. Amyloid, hypometabolism, and cognition in Alzheimer disease: an [11C]PIB and [18F]FDG PET study. Neurology. 2007; 68:501–508. [PubMed: 17065593]
9. Engler H, Forsberg A, Almkvist O, et al. Two-year follow-up of amyloid deposition in patients with Alzheimer's disease. Brain. 2006; 129:2856–2866. [PubMed: 16854944]

10. Lehmann M, Ghosh PM, Madison C, et al. Diverging patterns of amyloid deposition and hypometabolism in clinical variants of probable Alzheimer's disease. Brain. 2013; 136:844–858. [PubMed: 23358601]
11. Cohen AD, Price JC, Weissfeld LA, et al. Basal cerebral metabolism may modulate the cognitive effects of Abeta in mild cognitive impairment: an example of brain reserve. J Neurosci. 2009; 29:14770–14778. [PubMed: 19940172]
12. Jagust WJ, Landau SM, Shaw LM, et al. Relationships between biomarkers in aging and dementia. Neurology. 2009; 73:1193–1199. [PubMed: 19822868]
13. Mosconi L, Rinne JO, Tsui WH, et al. Amyloid and metabolic positron emission tomography imaging of cognitively normal adults with Alzheimer's parents. Neurobiol Aging. 2013; 34:22–34. [PubMed: 22503001]
14. Zhou Y, Resnick SM, Ye W, et al. Using a reference tissue model with spatial constraint to quantify [11C]Pittsburgh compound B PET for early diagnosis of Alzheimer's disease. Neuroimage. 2007; 36:298–312. [PubMed: 17449282]
15. Meyer PT, Hellwig S, Amtage F, et al. Dual-biomarker imaging of regional cerebral amyloid load and neuronal activity in dementia with PET and 11C-labeled Pittsburgh compound B. J Nucl Med. 2011; 52:393–400. [PubMed: 21321269]
16. Resnick SM, Goldszal AF, Davatzikos C, et al. One-year age changes in MRI brain volumes in older adults. Cereb Cortex. 2000; 10:464–472. [PubMed: 10847596]
17. Morris JC. The Clinical Dementia Rating (CDR): current version and scoring rules. Neurology. 1993; 43:2412–2414.
18. Driscoll I, Resnick SM, Troncoso JC, An Y, O'Brien R, Zonderman AB. Impact of Alzheimer's pathology on cognitive trajectories in nondemented elderly. Ann Neurol. 2006; 60:688–695. [PubMed: 17192929]
19. Kawas C, Gray S, Brookmeyer R, Fozard J, Zonderman A. Age-specific incidence rates of Alzheimer's disease: the Baltimore Longitudinal Study of Aging. Neurology. 2000; 54:2072–2077. [PubMed: 10851365]
20. Diagnostic and Statistical Manual of Mental Disorders: Third Edition, rev, DSM-III-R. Washington, D.C.: American Psychiatric Association; 1987.
21. McKhann G, Drachman D, Folstein M, Katzman R, Price D, Stadlan EM. Clinical diagnosis of Alzheimer's disease: report of the NINCDS-ADRDA Work Group under the auspices of Department of Health and Human Services Task Force on Alzheimer's Disease. Neurology. 1984; 34:939–944. [PubMed: 6610841]
22. Price JC, Klunk WE, Lopresti BJ, et al. Kinetic modeling of amyloid binding in humans using PET imaging and Pittsburgh Compound-B. J Cereb Blood Flow Metab. 2005; 25:1528–1547. [PubMed: 15944649]
23. Zhou Y, Endres CJ, Brasic JR, Huang SC, Wong DF. Linear regression with spatial constraint to generate parametric images of ligand-receptor dynamic PET studies with a simplified reference tissue model. Neuroimage. 2003; 18:975–989. [PubMed: 12725772]
24. Lopresti BJ, Klunk WE, Mathis CA, et al. Simplified quantification of Pittsburgh Compound B amyloid imaging PET studies: a comparative analysis. J Nucl Med. 2005; 46:1959–1972. [PubMed: 16330558]
25. Beason-Held LL, Kraut MA, Resnick SM. I. Longitudinal changes in aging brain function. Neurobiol Aging. 2008; 29:483–496. [PubMed: 17184881]
26. Yang X, Beason-Held L, Resnick SM, Landman BA. Biological parametric mapping with robust and non-parametric statistics. Neuroimage. 2011; 57:423–430. [PubMed: 21569856]
27. Yang X, Beason-Held L, Resnick SM, Landman BA. Robust biological parametric mapping: an improved technique for multimodal brain image analysis. Proc Soc Photo Opt Instrum Eng. 2011; 7962:79623X.
28. Casanova R, Srikanth R, Baer A, et al. Biological parametric mapping: A statistical toolbox for multimodality brain image analysis. Neuroimage. 2007; 34:137–143. [PubMed: 17070709]
29. Fox, J. Robust Regression An R and S-PLUS Companion to Applied Regression. Thousand Oaks, CA: Sage Publications, Inc.; 2002.

30. Fodero-Tavoletti MT, Rowe CC, McLean CA, et al. Characterization of PiB binding to white matter in Alzheimer disease and other dementias. J Nucl Med. 2009; 50:198–204. [PubMed: 19164220]

31. Yotter RA, Doshi J, Clark V, et al. Memory decline shows stronger associations with estimated spatial patterns of amyloid deposition progression than total amyloid burden. Neurobiol Aging. 2013; 34:2835–42. [PubMed: 23859610]

32. Blomquist G, Engler H, Nordberg A, et al. Unidirectional influx and net accumulation of PIB. Open Neuroimag J. 2008; 2:114–125. [PubMed: 19526073]

33. Yang X, Lauzon CB, Crainiceanu C, Caffo B, Resnick SM, Landman BA. Biological parametric mapping accounting for random regressors with regression calibration and model II regression. Neuroimage. 2012; 62:1761–1768. [PubMed: 22609453]

34. McNamee RL, Yee SH, Price JC, et al. Consideration of optimal time window for Pittsburgh compound B PET summed uptake measurements. J Nucl Med. 2009; 50:348–55. [PubMed: 19223409]

35. Zhou Y, Sojkova J, Resnick SM, Wong DF. Relative equilibrium plot improves graphical analysis and allows bias correction of standardized uptake value ratio in quantitative 11C-PiB PET studies. J Nucl Med. 2012; 53:622–8. [PubMed: 22414634]

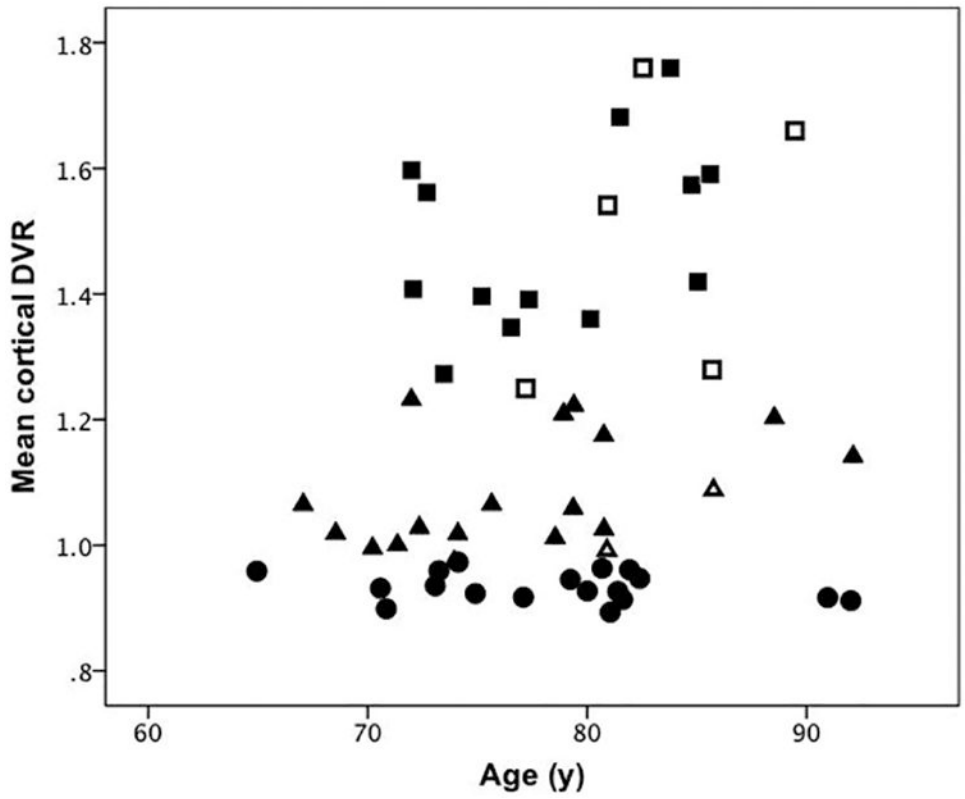

Figure 1. Distribution of cortical DVR values by tertiles

Upper tertile: squares. Middle tertile: triangles. Lower tertile: circles. Full symbols indicate individuals with CDR=0; open symbols represent individuals with CDR=0.5. CDR: Clinical Dementia Rating Scale

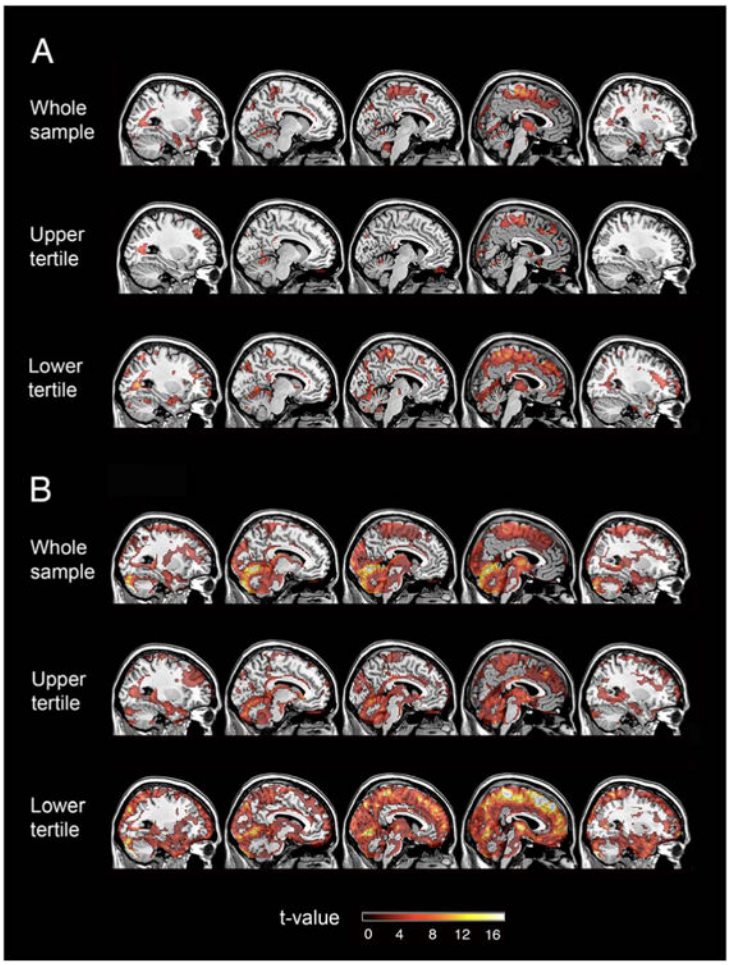

Figure 2. Positive associations between DVR, CBF, and R_1

(A) Positive associations between CBF and DVR (B) Positive associations between R_1 and DVR. CBF: cerebral blood flow. DVR: distribution volume ratio. R_1: influx rate constant

Table 1

Demographic, Genetic, and Cognitive Data

	Whole sample	Lower tertile	Middle tertile	Upper tertile	p-value
N	55	18	19	18	
Age (yrs)	78.5 (6.3)	78.3 (6.8)	77.4 (6.7)	79.8 (5.4)	0.34†
Sex - Males No. (%)	31 (56.4%)	11 (61.1%)	7 (36.8%)	13 (72.2%)	0.10‡
Race - White No. (%)	48 (87.3%)	17 (94.4%)	14 (73.7%)	17 (94.4%)	0.19‡
Education (yrs)	16.9 (2.3)	16.4 (2.3)	17.6 (1.8)	16.6 (2.6)	0.23†
CDR = 0.5 No. (%)	7 (12.7%)	0 (0%)	2 (10.5%)	5 (27.8%)	0.004*
ApoE4 carrier No. (%)	16 (29.1%)	1 (5.6%)	5 (26.3%)	10 (55.6%)	0.004*

Values represent mean (SD) unless otherwise indicated. CDR: Clinical dementia rating scale. ApoE4: Apolipoprotein E4.

† Kruskal Wallis test;

‡ Fisher exact test

Table 2
Global and regional distribution volume ratios (DVRs)

DVR	Whole sample	Lower tertile*	Middle tertile	Upper tertile*
N	N=55	N=18	N=19	N=18
Mean cortical DVR	**1.17(0.26)**	0.93(0.02)	**1.08(0.09)**	**1.49(0.16)**
Orbitofrontal gyrus	1.09(0.27)	0.86(0.04)	0.1(0.14)	1.40(0.19)
Prefrontal gyrus	1.11(0.29)	0.86(0.04)	1.02(0.13)	1.46(0.19)
Superior frontal gyrus	1.20(0.34)	0.90(0.04)	1.08(0.14)	1.61(0.22)
Parietal lobe	1.14(0.24)	0.92(0.05)	1.07(0.08)	1.42(0.19)
Medial temporal gyrus	1.01(0.09)	0.95(0.07)	1.01(0.06)	1.06(0.11)
Lateral temporal gyrus	1.13(0.24)	0.93(0.03)	1.05(0.12)	1.41(0.19)
Occipital gyrus	1.08(0.13)	0.99(0.06)	1.06(0.07)	1.19(0.15)
Anterior cingulate gyrus	1.27(0.34)	0.97(0.07)	1.17(0.18)	1.67(0.23)
Posterior cingulate gyrus	1.32(0.35)	1.02(0.06)	1.19(0.1)	1.76(0.23)

Data are presented as mean (SD) distribution volume ratio.

*All DVR measures are significantly higher in the upper tertile than the lower tertile ($p<0.005$). Data in bold indicate greater than DVR positivity cut-off of 1.062 for cDVR, indicating more than minimal Aβ.